Nonresonant and Resonant Surface-Enhanced Raman Scattering of N-Ethyl-N-(2-hydroxyethyl)-4-(4-nitrophenylazo) Aniline in Poly(methyl methacrylate) on Ag Films with Surface Roughness

Nonresonant and resonant surface-enhanced Raman scattering of *N*-ethyl-*N*-(2-hydroxyethyl)-4-(4-nitrophenylazo) aniline in poly (methyl methacrylate) on Ag films with surface roughness

Ayaka Izumi, Kentaro Kumaoka, Masaru Shimomura, and Atsushi Sugita

Faculty of Engineering, Shizuoka University, 3-5-1 Johoku, Naka-ku, Hamamatsu, Shizuoka 432-8561, Japan

sugita.atsushi@shizuoka.a.cjp

Abstract

Nonresonant and resonant surface-enhanced Raman scatterings (SERS and SERRS) were studied for *N*-ethyl-*N*-(2-hydroxyethyl)-4-(4-nitrophenylazo) aniline (Disperse Red 1, or DR1) in poly (methyl methacrylate) on Ag films with surface roughness. DR1 is the chromophore that consists of azobenzene bridged between the electron-donating amine and electron-accepting nitro groups, and it has attracted great attentions because of its large molecular hyperpolarizability. The DR1 hybridized with metal nanoparticles or nanostructures is promising as the building block for nonlinear plasmonics. Our experimental results demonstrated that the Raman cross sections were highly enhanced both at the molecular nonresonant and resonant excitation wavelengths. The spectroscopic properties of SERRS were taken from resonant Raman (RR), and the enhanced RR cross sections were attributed to electromagnetic enhancements due to surface plasmons (SP). The SERS spectrum was also similar to the RR spectrum, rather than the nonresonant Raman (NR) spectrum, even at the molecular nonresonant excitations. The diagram of energy levels was drawn for the DR1/Ag interfaces by using the spectroscopic data of ultraviolet-visible linear absorption and ultraviolet photoelectron. The enhanced NR cross sections were explained in terms of the electromagnetic enhancements, as well as the metal-to-molecular charge-transfer, by using the energy diagram.

Keywords: SERS, Nonlinear optical chrmophores, Metal-to-molecule charge-transfer

1. Introduction

Considerable attention has been drawn to optical properties of plasmon-molecule hybrid systems[1-4]. The surface plasmons are collective oscillations of conducting electrons on metal surfaces[5,6]. Surface plasmon generation brings intense optical fields into the vicinity of the metal nanoparticles or nanometrically structured metal surfaces. The intense and confined optical fields due to the surface plasmons are useful for boosting light-molecular interactions on the metal surfaces. The stronger plasmon-molecule couplings even create hybridized molecular electronic states due to Rabi splitting [7,8]. Plasmon-mediated photo-excitations highly elevate the Raman scattering cross section[9-12], fluorescence quantum yield[13-15] and infrared absorption intensity [16,17]. The enhanced sensitivity of Raman scattering, fluorescence and infrared absorption spectroscopies are used in chemical and biosensing technologies for small volumes of the molecules or even single molecules[18,19].

Hybridizations with metal nanoparticles have been investigated for a wide variety of molecules thus far. Azobenzene and its derivatives are some of the most important optical molecules among them[20-25]. The fundamental structure of azobenzene consists of two phenyl rings bridged with N=N groups. The compounds have trans- and cis-isomers, which are mutually transformable under the photo-irradiation[26,27]. The photo-induced trans-cis and cis-trans isomerizations undergo material motions in mesoscopic and even macroscopic spatial scales. By taking advantage of the opto-mechanical conversion effects, the formation of surface reliefs and molecule-based motors was demonstrated under light exposures. The photo-induced isomerization of azobenzene also controls and tunes the localized surface plasmon resonance frequency in the assembly of azobenzene-cores and metal nanoparticle-shells[24]. These technologies are promising for photoswitching systems in the micro- and nanophotonics fields.
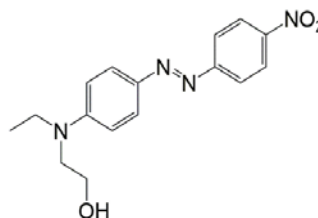

Figure 1 Structure of DR1.

Disperse Red 1 (DR1), or *N*-ethyl-*N*-(2-hydroxyethyl)-4-4-(nitrophenylazo) aniline, is a compound consisting of an electron donating ethyl hydroxylethyl amine and an electron accepting nitro group bridged by the azobenzene (Fig. 1)[28-30]. It possesses large molecular nonlinearity due to the photo-induced intramolecular charge-transfer effects from the electron donor to the electron acceptor. The DR1 dispersed in amorphous polymers exhibited second harmonic generations (SHG) and electro-optic effects after being electrically poled. The materials are useful for optical frequency convertors, electro-optic devices or optical modulators.

We examined the SHG effects for the DR1 doped in poly (methyl methacrylate) (PMMA) (DR1-PMA) grown on the Ag thin films at the surface plasmon resonances in our previous study[31]. In the study, the surface plasmons were generated by attenuated total reflections in Kretchman geometry. The Ag films themselves possessed surface nonlinearities, and they emitted enhanced SHG at the surface plasmon resonances. Our research demonstrated that the SHG signals emitted by DR1-PMMA coated on Ag films were approximately 7 times higher

than those from the pristine Ag films. The results indicated that the hybridizations of metal nanostructures with nonlinear optical molecules are suitable for boosting the nonlinearities of the plasmonic metal surfaces. However, the molecule-plasmon or molecule-metal interactions responsible for the enhanced nonlinearities remain unclear.

In this article, we report surface-enhanced Raman scattering spectroscopy of DR1 in PMMA. The surface plasmons were generated by using the surface roughness of the Ag thin films on a SiO$_2$ substrate. The light sources with two different excitation wavelengths were prepared to obtain the Raman signals. Both of the excitation wavelengths were able to resonantly excite the surface plasmons on the Ag surfaces. However, one of the excitation wavelengths was resonant to the molecular electronic transitions of the DR1, while the other was not. Thus, the surface enhanced Raman scattering (SERS) and the surface-enhanced resonant Raman scattering (SERRS) signals were obtained by using these two light sources.

For comparison, we examined the normal molecular nonresonant (NR) and resonant Raman (RR) spectroscopies using the DR1-PMMA films grown directly on the SiO$_2$ substrates. Energy levels of the DR1 with respect to Fermi level of the Ag were also determined by investigating ultraviolet-visible (UV-VIS) absorption and ultraviolet photoelectron (UPS) spectroscopies. We addressed the probable molecule-metal interactions responsible for the enhancements in the Raman cross sections by using the energy diagram. The comprehensive studies unraveled the vibronic coupling in DR1 on Ag surfaces under the surface plasmon resonances.

2. Experimental

The Ag films were prepared on the SiO$_2$ substrates by the vacuum deposition method. The shots of Ag were evaporated with a resistive heater. The Ag film thickness was 10 nm. The morphology of the Ag thin films was polycrystalline, which contained an assembly of island-shaped microcrystallites with 20-50 nm particle sizes. DR1 and PMMA were purchased from Aldrich Company and they were used without further purifications. The average molecular weight of the PMMA was $M_w=1.2 \times 10^5$. The DR1-PMMA films were prepared with a spin coating method. The mixture of the DR1 and PMMA was dissolved in propionitrile. The concentration of DR1 in the mixture was 10 w%. A drop of the solutions was spanned on the Ag films.

The DR1-PMMA layers with a 5 nm-thickness were grown on the Ag films on the SiO$_2$ substrates (DR1-PMMA/Ag/SiO$_2$ structure) for the SERS and SERRS spectroscopies, while the DR1-PMMA layers with 500 nm were grown on the SiO$_2$ substrates (DR1-PMMA/SiO$_2$ structure) for the NR and RR spectroscopies. The pristine PMMA films, where the chromophores were not dispersed, were also grown on the Ag/SiO$_2$ and SiO$_2$ substrates (PMMA/Ag/SiO$_2$ and PMMA/SiO$_2$ structures) for measuring the background signals due to the Ag and PMMA. The film thicknesses were the same as their counterpart samples. The Ag films dip-coated in the solutions of the DR1 were also prepared as references (DR1/Ag/SiO$_2$ structure). The DR1 was dissolved in propionitrile without mixing the PMMA. After being dipped for 30 min, the films were rinsed twice in the propionitrile and dried.

The Raman signals were studied at room temperature using a microscopic Raman spectrometer (NRS-700, JASCO). The wavelengths of the unpolarized excitation lights was 532 nm for RR and SERRS or 785 nm for NR and SERS. The power of the excitation lights was 0.1mW for 532 nm and 1.3mW for 785 nm. The light exposure times were 60 - 180 sec, depending on the samples. In the later discussion, the Raman spectra are displayed

after being normalized with respect to the polymer film thickness, excitation light power and the light exposure times.

The UV-VIS absorption spectra were measured by using the home-built system, in which the light source was a xenon-lamp (L2175, Hamamatsu Photonics K. K.). The white lights were spectrally resolved with a monochronometer (SP150, Acton Research Co.), and they were detected by a Si photodiode (2032, Newport Co.) after transmitting the samples. The energy levels of the molecules were determined by the UPS spectrometer (AXIS Ultra, KRATOS analytical Ltd.). The UV excitation light source was HeIα line (21.2 eV) of a helium lamp. The measurements were performed with the DR1/Ag/SiO$_2$ structure. The UPS spectra of the bare Ag surfaces were also measured with Ag/SiO$_2$ substrates as a references. The surfaces of the samples were etched by argon cluster ion beams.
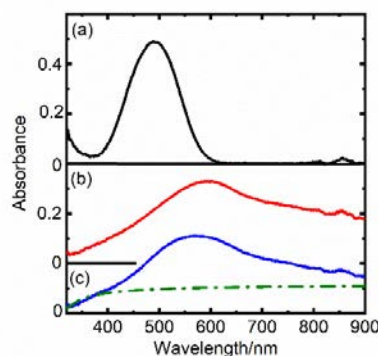
3. Results and Discussion

Figure 2 (a) UV-VIS absorption spectrum of (a) DR1-PMMA/SiO$_2$ structure. (b) and (c) are DR1-PMMA/Ag/SiO$_2$ and PMMA/Ag/SiO$_2$ structures, respectively. The dash-dotted curve in (c) are the absorption coefficients of Ag film referred from [34].

Fig. 2(a) presents the UV-VIS absorption spectrum of the DR1-PMMA/SiO$_2$ structure. The strong absorption peak at 485 nm is in agreement with the spectrum of the trans-isomers of DR1 from previous studies; it was assigned to the π-π* transition with charge-transfer character[32,33].

Fig. 2(b) and (c) are the linear absorption spectra of the DR1-PMMA/Ag/SiO$_2$ and PMMA/Ag/SiO$_2$ structures, respectively. The absorption spectrum of Ag is referenced in the literature[34] and is also shown in (c) by a dashed curve. In both of the spectra, the broad absorption band due to the surface plasmons, which were extended at ~400-900nm, was superposed on the flat structureless absorption bands for the Ag in the literature. The peak positions for the DR1-PMMA/Ag/SiO$_2$ and PMMA/Ag/SiO$_2$ structures were ~594 nm and ~568 nm, respectively. The red shift of the former with respect to the latter was probably due to the coupling between the molecular excitons and plasmons[7,8]. The hybridizations reduced the oscillation frequency of the surface plasmon polarizations on the Ag surface.

On the other hand, no new band due to the metal-molecule complex structure was found in the spectrum. In the present study, two excitation light sources at 532 nm and 785 nm were employed. The former resonantly excited the π-π* molecular transitions of the DR1, as well as the surface plasmon polarizations on the Ag surfaces. The latter was only resonant to the surface plasmon polarizations.

Fig. 3 shows the UPS spectrum of the DR1 on the Ag surfaces along with that of the bare Ag surface. Fermi level of

the Ag, E_F, was determined from a rising edge of the spectrum. Here, the spectra were plotted as a function of the energy relative to E_F. There are two peaks in the UPS spectrum of the DR1. The peaks at 2.0 and 2.8 eV might be assigned to the HOMO and HOMO-1 levels, respectively.
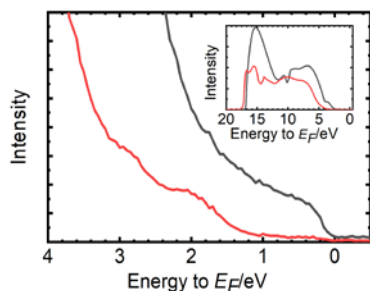

Figure 3 UPS spectrum of DR1 on Ag surfaces (red) and bare Ag surfaces (black curve). The inset is the plot up to 20 eV.

The previous one- and two-photon absorption spectroscopies demonstrated that the energy separations between the HOMO and HOMO-1 levels of the DR1 was as small as 0.1-0.3 eV[32]. It was much smaller than the ~0.8 eV-separation between the two UPS peaks. The quantum chemical calculations also supported the evidence that the HOMO and HOMO-1 levels were close to each other[35,36]. It was concluded that the component at 2.0 eV in the UPS spectrum was attributed to both of the HOMO and HOMO-1 levels, and the component at 2.8 eV was attributed to the HOMO-2 level. The two bands due to the HOMO and HOMO-1 levels could not be separated sufficiently with the energy resolution of the present spectrometer.
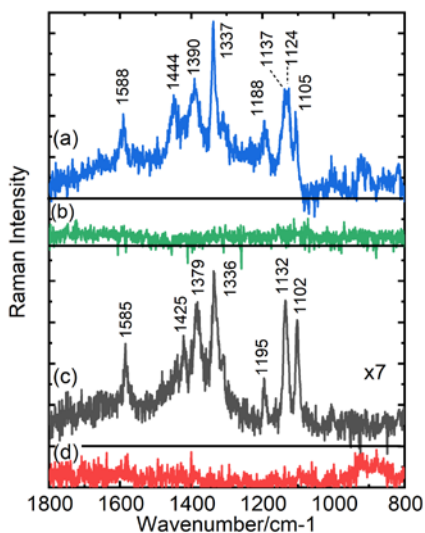

Figure 4 (a) RR spectrum of DR1-PMMA and (b) PMMA at 532 nm-excitation light and (c) NR spectrum of DR1-PMMA and (d) PMMA excited at 785 nm-excitation light. The data (c) and (d) were displayed after magnifying 7 times.

Fig. 4(a) and (c) show the NR and RR spectra obtained by pumping the DR1-PMMA/SiO$_2$ structures at 785 nm and 532 nm, respectively. The Raman spectra were also studied for the PMMA/SiO$_2$ structures at both of the excitation wavelengths and they were also shown in Fig. 4(b) and (d), respectively. The exposure times were 180 sec. The Raman spectra of the

references contained only weak broad and structureless signals. Thus, the Raman bands in the DR1-PMMA/SiO$_2$ structures were attributed to the DR1 chromophore.

There are prominent bands at 1102, 1132, 1195, 1336, 1379, 1425, and 1585 cm^{-1} in the NR spectrum. The vibrational structures of the several substituted azobenzene derivatives, including DR1, have been studied extensively[37-43]. The assignments of the bands were supported by the quantum chemical calculations, especially the density functional theory (DFT). In reference to these previous studies, the Raman bands are assigned to as in Table 1.

Table 1: Wavenumbers (cm^{-1}), enhancement factors, and assignments of NR, RR, SERS, and SERRS of DR1 in PMMA

NR	RR		SERS		SERRS		Assignments
ν_{NR}	ν_{RR}	EF_{RR}	ν_{SERS}	EF_{SERS}	ν_{SERRS}	EF_{SERRS}	
1102	1105	5	1102	500	1103	1400	phenyl-NO$_2$ stretch
	1124		1120		1123	2900	phenyl-NN stretch (cis)
1132	1137	4	1134	900	1138	2800	phenyl-NN stretch
1195	1188	6	1186	1300	1187	3300	CH bend
1336	1337	8	1336	200	1336	1500	NO$_2$ stretch
1379	1390	6	1397	1100	1397	5300	N=N stretch
1425	1444	13	1450	2000	1442	3000	C-C stretch
1585	1588	6	1587	1200	1593	7200	C-C stretch

The bands other than those at 1102 and 1336 cm^{-1} were also observed from the Raman spectra of the azobenzene trans-isomers[37-39]. Furthermore, the frequency positions of the bands at 1132, 1195 and 1585 cm^{-1} did not change substantially upon substituting the nitro groups as well as [N-ethyl-(N-hydroxylethyl)] amines in the azobenzene[40]. The bands at 1132 and 1195 cm^{-1} were attributed to the phenyl-NO$_2$ stretching and in-plane CH bending modes, respectively. The band at 1585 cm^{-1} was related to the C-C stretching of the NO$_2$ substituted phenyl groups.

The band at 1379 cm^{-1} was mainly due to the N=N stretching. The band appeared at 1440 cm^{-1} in the unsubstituted azobenzene tans-isomer[37-39]. The observed frequency position for the DR1 was by 60cm^{-1} lower than that of the azobenzene trans-isomer. The assignment was justified from the frequency shift of the bands upon the isotopic substitutions of the ^{15}N in the azo moieties. The previous DFT analysis demonstrated that the frequency of the band was largely red-shifted upon the isotropic substitutions[40]. The amount of the red shift was approximately 10 cm^{-1} against the mono-substitution and 30 cm^{-1} against the di-substitution of ^{15}N.

The band at 1425 cm^{-1} was mostly due to the C-C stretching in the phenyl parts. The frequency position was close to that due to the N=N stretch of the parent unsubstituted azobenzene. The DFT calculation indicated that the frequency position of the band did not change even after isotopically substituting the ^{15}N in the azo moiety[40]. Hence, the potential energy distribution due to the N=N stretches was negligible for the band.

The bands at 1102 and 1336 cm^{-1} were not found in the spectrum of the azobenzene trans-isomer. They were not found in the spectrum of 4-dimethylamino-azobenzene, in which the

azobenzene was substituted by the dimethylamine. On the other hand, they were found in the spectrum of the 4-nitro-azobenzene, in which the azobenzene was substituted by the nitro group[40,41]. Therefore, these bands were related to the vibrations of the NO_2 groups. The former was due to the phenyl-NO_2 stretching, while the latter was due to the symmetric stretching of the NO_2.

In the RR spectrum, the Raman signal intensities were enhanced at most of the bands observed in the NR spectrum. The enhancements due to the molecular resonances were evaluated by using the factor $EF_{RR,v} = I_{RR,v}/I_{NR,v}$, where $I_{RR,v}$ and $I_{NR,v}$ are the Raman intensities at v cm^{-1} in the RR and NR spectra, respectively. The factors were $EF_{RR,v}$~5-7 at most of the bands.

The polarizabilities on the molecular resonant conditions are expressed with the summations of Franck-Condon and vibronic coupling terms. As is the case with the azobenzene, the HOMO and HOMO-1 levels of DR1 were the n- and π-orbitals, respectively, and the excitation to the $S_2(ππ^*)$ state was the lowest optically-allowed transition. Since the S_2 and $S_1(nπ^*)$ states were close to each other, the fast internal conversion occurred from the former to the latter within 0.2 ps[36]. Furthermore, the potential energy surfaces of the S_1 and S_0 states were conically intersected along the out-of-plane CNNC torsional motions in DR1. The n-π* and π-π* transitions were coupled through torsional motions. The Raman modes due to the motions may exhibit the vibronic coupling characters. All of the modes observed in the study, however, were due to the in-plane motions, and they should be classified into Franck-Condon term.

The RR spectrum behaved differently from the NR in three ways. First, the band due to the N=N stretching at 1379 cm^{-1} in the NR spectrum was largely blue-shifted to 1390 cm^{-1} in the RR spectrum. The blue-shift was probably due to Raman dispersion effects, where the positions of the Raman bands were shifted to the higher frequencies as the excitation photon energies were higher. The phenomena were found in the conjugated systems, such as C=C stretching modes in poly thiophene and poly pyrrole or the C-N stretching in poly aniline [44-46]. The phenomena can be explained in terms of the conjugation length of the molecules, with shorter lengths found in resonance with higher excitation photon energy.

In the present DR1/PMMA system, the DR1 molecules were able to accept different N=N conjugation lengths in the randomly oriented amorphous PMMA chains. The 532 nm-excitation lights were resonant to the DR1 molecules with shorter conjugation length than the 785 nm-lights.

Second, the mode at 1444 cm^{-1} due to the C-C stretching in the phenyl rings increased the enhancement factors more than the other modes. The band was barely seen in the NR spectrum, while it was clearly found in the RR spectrum. The enhancement factor of the band was $EF_{RR,1444}$~13, which was much larger than $EF_{RR,v}$~5-7 for the other bands. Third, the band at 1124 cm^{-1} in the RR spectrum was not seen in the NR spectrum. The band may be attributed to the coupling between N-phenyl stretching and in-plane CH bending modes of the cis-isomers [38,39].

The enhanced Raman modes other than 1124 cm^{-1} may be also attributed to the cis-isomers produced by the photo-isomerization reaction. The previous studies presented that, other than the band at 1123 cm^{-1}, the Raman spectrum of the cis-isomers were almost silent in the regions 800-1800 cm^{-1}, except the weak bands at ~1510 and ~1590 cm^{-1} [44,45]. Because of the reductions in the point symmetries of the vibration coordinates through the photo-isomerization, the Raman active modes in the trans-geometry became inactive in the cis-geometry. Hence, the enhanced Raman signals were mostly attributed to the trans-isomers in the S_0 state.

The DR1 molecules may be also photo-reduced and the NO_2 groups were converted to the NH_2 group. The previous

studies found the band at ~1124 cm^{-1} from the photo-reduced DR1 molecules[47,48]. In the present state, we cannot conclude that either of the assignments are correct from the limited information.

The SERS spectra of the DR1-PMMA/Ag/SiO$_2$ and the PMMA/Ag/SiO$_2$ structures are shown in Fig. 5(a). The SERS of the DR1/Ag/SiO$_2$ structure is shown in Fig 5(b) along with the scattering spectrum from the Ag/SiO$_2$ structure, in which the DR1 chromophores were not adsorbed at all. The NR spectrum, which is the same as that in Fig. 3, is also shown in Fig. 5(c). The exposure time was 60 sec.

The SERS spectrum of the DR1-PMMA was essentially the same as that of DR1 on the Ag surfaces. The signal intensities of the former was approximately 30% of those of the latter. Hence, the SERS signals of the DR1-PMMA was mostly due to the molecules directly adsorbed on the Ag surface. In the DR1-PMMA system, the polymeric chains of the PMMA were also adsorbed on the Ag surfaces. Because of the existence of the PMMA chain, the SERS intensities in the DR1-PMMA system were lower than those in DR1 on the Ag surfaces.

The SERS enhancement factors were evaluated by using the ratio $EF_{SERS,v} = I_{SERS,v}/I_{NR,v}$, where $I_{SERS,v}$ and $I_{NR,v}$ are the Raman intensities at v cm^{-1} in the SERS and NR spectra, respectively (Table 1). The bands due to the azobenzene moieties achieved greater enhancements than those related to the NO_2 groups. The factors related to the azobenzene moieties were $EF_{SERS,1120}=9.0\times10^2$, $EF_{SERS,1186}=1.3\times10^3$, $EF_{SERS,1397}=1.1\times10^3$, $EF_{SERS,1450}=2.0\times10^3$ and $EF_{SERS,1587}=1.2\times10^3$. The factors for the band related to the NO_2 group were $EF_{SERS,1102}=5.0\times10^2$ and $EF_{SERS,1336}=2.0\times10^2$.
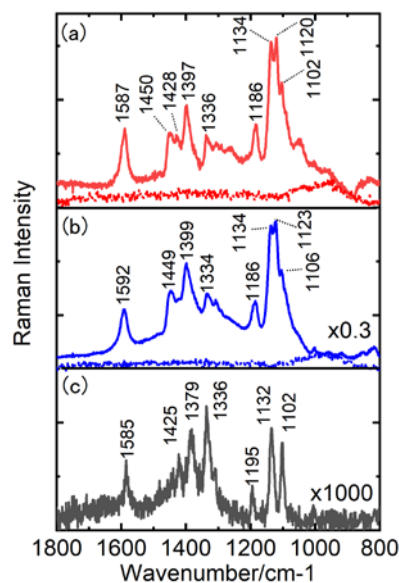

Figure 5 (a) SERS spectra of DR1-PMMA (solid) and PMMA (dashed curve) at 785 nm-excitation light wavelength. (b) SERS spectra of DR1(solid), the pristine Ag (dashed curve), and (c) NR spectra of DR1-PMMA at the same wavelength. The data (b) and (c) were displayed after magnifying 0.3 and 1,000 times, respectively.

The spectroscopic features of the SERS were similar to those of the RR, rather than those of the NR. First, the band due to the N=N stretching was located at 1397 cm^{-1}. It was blue shifted by 18 cm^{-1} with respect to its counterpart in the NR spectrum probably because of the Raman dispersion effects. Second, the intensity of the band at 1450 cm^{-1} was clearly visible

in the SERS spectra and its enhancement factor was much higher than that of the others. Third, the band at 1120 cm^{-1} due to either the cis-isomers or the photo-reduced molecules was found in the SERS spectrum, which was found in the RR but not in the NR spectrum.

The enhanced Raman signals may be attributed to not only propagating surface plasmon polaritons on the metal surfaces but localized surface plasmons due to the hot spots among the aggregates of the Ag particles. The latter effects were characterized with the spectral modulations; that is, the relative signal intensities of the Raman modes greatly differed among the observation positions on the samples[49]. It was because of the sensitive changes in the spectral shape of the localized surface plasmon against the morphologies of the aggregates of the particles. That kind of spectral modulations were not observed in the present study, and the observed SERS were mostly due to the localized surface plasmon resonances.

Fig. 6(a) show the SERRS spectrum of DR1-PMMA/Ag/SiO$_2$ and PMMA/Ag/SiO$_2$ structures. The SERRS of the DR1/Ag/SiO$_2$ structure is shown along with the scattering spectrum of the Ag/SiO$_2$ structure in Fig. 6(b). The RR spectrum of the DR1-PMMA are also shown in Fig 6(c). The exposure time was 60 sec. The SERRS spectrum of the DR1-PMMA/AgSiO$_2$ structure was quite similar to that of the DR1/Ag/SiO$_2$ structure. Like in the case of the SERS, the SERRS signals of the DR1-PMMA were mostly due to the molecules directly adsorbed on the Ag surfaces. In addition, it inherited the characteristics from the RR. The positions of the main bands in the SERRS were essentially the same as those in the RR. The band at 1379 cm^{-1} in the NR was blue-shifted to 1397 cm^{-1} in the SERRS. In addition, the band due to either the cis-isomer or the photo-reduced molecules was found at 1123 cm^{-1}.

were $EF_{SERRS,1138}=2.8\times10^3$, $EF_{SERRS,1187}=3.3\times10^3$, $EF_{SERRS,1397}=5.3\times10^3$, $EF_{SERRS,1442}=3.0\times10^3$ and $EF_{SERRS,1593}=7.2\times10^3$, while the factors for the latter were $EF_{SERRS,1103}=1.4\times10^3$ and $EF_{SERRS,1336}=1.5\times10^3$.

In summarizing the experimental results so far, both of the SERS and SERRS spectra revealed features similar to the RR. The surface enhancements of the Raman cross sections at the molecular resonance were explained by electromagnetic mechanisms; the strong local optical fields due to the surface plasmon resonances were coupled with the molecules near the metal surfaces. In the SERRS spectrum, the Raman bands related to the azobenzene moieties increased the enhancements more than two times those related to NO$_2$ moieties. As mentioned above, the UV-VIS absorptions of the DR1 molecules were attributed to π-π^* transition in the azobenzene moieties. The surface plasmon enhanced optical fields promoted Franck-Condon molecular transitions related to the conjugated orbitals of the azobenzene moieties.

Additionally, the characteristics of the SERS spectrum were similar to those of the RR, rather than the NR spectrum. Although the excitation photon energy was far from the molecular resonances, the resonance to the electronic excited states accounted for the surface enhancements of the Raman signals. The previous study claimed that there was a potential barriers as high as 0.3 eV between trans and cis-conformations in the potential surface of the S$_0$ state [35,36]. The trans-cis isomerization was less likely to occur by thermal pathway. The electromagnetic mechanism alone cannot explain the enhancements of the Raman cross sections at the molecular off-resonance conditions. The charge-transfer resonance was taken into account for explaining the spectroscopic behaviors [49-51].

There are two probable charge-transfer pathways associated with the enhancements of the Raman scattering cross sections. The first pathway is molecule-to-metal transfer from the occupied molecular electronic state E_I to the unoccupied levels in the conduction bands of the metals above E_F, the Fermi level of Ag. The second pathway is metal-to-molecule transfer from the occupied levels in the conduction bands of the metals below E_F to the unoccupied molecular electronic state E_K. In both cases, E_F has to be located between E_I and E_K. The former process occurs when the excitation photon energy $h\nu$ is higher than E_F-E_I. The latter occurs when the condition $h\nu > E_K$-E_F is satisfied.
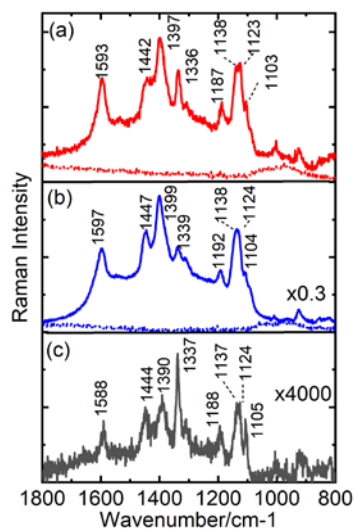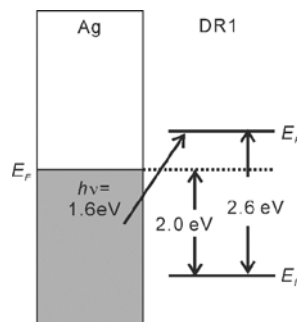

Figure 6 SERRS spectra of DR1-PMMA and PMMA (dashed curve) at 532 nm-excitation light wavelength. (b) SERRS spectra of DR1 and (c) RR spectra of DR1-PMMA at the same wavelength. The data (b) and (c) were displayed after magnifying 0.3 and 4,000 times, respectively.

The SERRS enhancement factors were evaluated by using the ratio $EF_{SERRS,\nu}=I_{SERRS,\nu}/I_{RR,\nu}$, where $I_{SERS,\nu}$ and $I_{RR,\nu}$ are the Raman intensities at ν cm^{-1} in the SERRS and RR spectra, respectively (Table 1). The enhancement factors of the modes related to the azobenzene moiety were much higher than those related to the NO$_2$ moieties. The factors for the former modes

Figure 7 Energy diagram of molecule-metal hybrid system. E_I and E_K are the molecular occupied and unoccupied electronic levels of DR1, while E_F is Fermi level of Ag. $h\nu$ is the photon energy for nonresonant Raman excitation.

The energy diagram of the molecule-metal hybrid system is drawn in Fig. 7. The position of the occupied molecular electric state of the DR1 was located at E_I~2.0 eV below E_F of Ag from the UPS spectrum in Fig. 3. The molecular electron transition energy was determined by the UV-VIS absorption

spectrum in Fig. 2(a) and it was E_K-E_I=2.6 eV, corresponding to the absorption peak wavelength of 485 nm. Hence, E_K were located above ~0.6 eV with respect to E_F.

The excitation photon energy for the nonresonant Raman excitation was $h\nu$=1.6 eV, corresponding to a 785 nm-wavelength. It was able to resonantly excite the metal-to-molecule charge-transfer transition, or E_K-E_F~0.6 eV, since the condition $h\nu > E_K - E_F$ was satisfied. Therefore, the metal-to-molecule charge-transfer mechanism contributed to the enhancements of the Raman cross sections at the molecular off-resonant excitations in addition to the electromagnetic effect due to the surface plasmon enhanced optical fields. On the other hand, $h\nu$ is smaller than $E_F - E_I$ ~ 2.0 eV and the molecule-to-metal charge transfer was less likely to occur.

Our previous study demonstrated that the NLO polymer made of the DR1-PMMA system was useful for enhancing the second-order nonlinearities on the Ag surfaces at the surface plasmon resonances. The enhanced SHG signals were obtained by using the 780 nm-excitation wavelength, which was nearly the same as the NR excitation source in the present study. The metal-to-molecule charge-transfer effects revealed by the present study may be responsible for the enhanced second-order nonlinearities in the NLO polymer/plasmonic metal hybrid systems.

4. Conclusions

In the study, the surface-enhanced Raman scatterings were examined for DR1, one of the most popular push-pull type NLO chromophores, in PMMA. The Raman excitations were performed both at the molecular on- and off-resonance conditions. The Raman modes were classified into two modes due to the azobenzene moieties and the NO_2 moieties in the electron acceptors. Compared with the NR spectra, the RR spectra increased the enhancements in the modes due to the azobenzene moieties than the NO_2 moieties. This was because the transition moments of the DR1 molecules were associated with the π-π* transitions in the azobenzene moieties. The spectroscopic features of the SERRS were in good agreements with those of the RR. The Raman enhancements were explained in terms of the electromagnetic enhancement mechanism. However, the spectroscopic features of the SERS were similar to those of the RR, rather than the NR. The enhancements of the Raman signals were attributed not only to the electromagnetic mechanism but also to the metal-to-molecule charge-transfer mechanism.

References

1. A. Spangenberg, R. Métivier, R. Yasukuni, K. Shibata, A. Brosseau, J. Grand, J. Aubard, P. Yu, T. Asahi, K. Nakatani, *Phys. Chem. Chem. Phys.* **2013**, 15, 9670.
2. M. Gruber, M. Mayr, T. Lampe, B.-C. Gallheber, B. J. Scholz, W. Bruetting, *Appl. Phys. Lett.* **2015**, 106, 083303.
3. A.-L. Baudrion, A. Perron, A. Veltri, A. Bouhelier, P.-M. Adam, R. Bachelot, *Nano Lett.* **2013**, 13, 282.
4. Y. Zhang, Z. Shuai, H. Zhou, Z. Luo, B. Liu, Y. Zhang, L. Zhang, S. Chen, J. Chao, L. Weng, Q. Fan, C. Fan, W. Huang, L.Wang, *J. Am. Chem. Soc.* **2018**, 140, 3988.
5. A. Hohenau, A. Leithner, F. R. Aussenegg, in *Surface Plasmon nanophotonics* (Eds. M. L. Brongersma, P. G. Kik), Springer, Dordrecht, **2007**, pp. 11-25.
6. R. Hooper, W. L. Barnes, in *Modern plasmonics,* (Eds. A. Maradudin, J. R. Sambles, W. L. Barnes.), Elsevier, Amsterdam, **2014**, pp. 37-74.
7. A. E. Schlather, N. Large, A. S. Urban, P. Nordlander, N. J. Halas, *Nano Lett.* **2013**, 13, 3281.
8. I. Väkeväinen, R. J. Moerland, H. T. Rekola, A. -P. Eskelinen, J. -P. Martikainen, D. -H. Kim, P. Törmä, *Nano Lett.* **2014**, 14, 1721.
9. M. Fleischmann, P. J. Hendra, A. J. McQuillan, *Chem. Phys. Lett.* **1974**, 26, 163.
10. M. Moskovits, *Rev. Mod. Phys.* **1985**, 57, 783.
11. K. Kneipp, H. Kneipp, I. Itzkan, R. R. Dasari, M. S. Feld, *Chem. Rev.* **1999**, 99, 2957.
12. L. Jensen, C. M. Aikens, G. C. Shatz, *Chem. Soc. Rev.* **2018**, 37, 1061.
13. K. H. Drexhage, *J. Lumin*, **1970**, 1-2, 693.
14. J. Kümmerlen, A. Leitner, H. Brunner, F. R. Aussenegg, A. Wokaun, *Mol. Phys.* **1993**, 80, 1031.
15. F. Tam, G. P. Goodrich, B. R. Johnson, N. J. Halas, *Nano Lett.* **2007**, 7, 496.
16. A. Hartstein, J. R. Kirtley, J. C. Tsang, *Phys. Rev. Lett.* **1980**, 45, 201.
17. M. Osawa, M. Ikeda, J. Phys. Chem. **1991**, 95, 9914.
18. H. Imada, K. Miwa, M. Imai-Imada, S. Kawahara, K. Kimura, Y. Kim, *Phys. Rev. Lett.* **2017**, 119, 013901.
19. W. Zhang, M. Caldarola, X. Lu, B. Pradhan, M. Orrit, *Phys. Chem. Chem. Phys.* **2018**, 20, 20468.
20. J. H. Yoon, S. Yoon, *Phys. Chem. Chem. Phys.* **2011**, 13, 12900.
21. A. Priimagi, A.Shevchenko, *J. Polym. Sci., Part B: Polym. Phys.* **2014**, 52, 163.
22. B. C. Galarreta, I. Rupar, A. Young, F. Lagugne-Labarthet, *J. Phys. Chem. C* **2011**, 115, 15318.
23. G. K. Joshi, K. N. Blodgett, B. B. Muhoberac, M. A. Johnson, K. A. Smith, R. Sardar, *Nano Lett.* **2014**, 14, 532.
24. E. S. Kristen, M. Jean-Yves, H. Bernard, L.-L. François, I. Elena, *ACS Appl. Mater. Interfaces*, **2015**, 7, 1932.
25. A. Natansohn, P. Rochon, *Chem. Rev.* **2002**, 102, 4139.
26. Y. Yu, M. Nakano, T. Ikeda, *Nature* **2003**, 425, 145.
27. T. Ikegami, Y. Kageyama, K. Obara, S. Takeda, *Angew. Chem. Int. Ed.* **2016**, 55, 8239.
28. H.L. Hampsch, J. Yang, G.K. Wong, J.M. Torkelson, *Macromolecules* **1988**, 21, 526.
29. T. Pliška, W. -R. Cho, J. Meier, A. -C. L. Duff, V. Ricci, A. Otomo, M. Canva, G. I. Stegeman, P. Raimond, F. Kajzar, *J. Opt. Soc. Am. B* **2000**, 17, 1554.
30. Y. Tu, Q. Zhang, H. Ågren, *J. Phys. Chem. B* **2007**, 111, 3591.
31. A. Sugita, K. Suto, T. Sato, A. Ono, W. Inami, Y. Kawata, S. Tasaka, *Proceedings of SPIE* **2013**, 8622, 86220B-7.
32. L. D. Boni, C. Toro, A. E. Masunov, F. E. Hernández, *J. Phys. Chem. A* **2008**, 112, 3886.
33. Toro, A. Thibert, L. D. Boni, A. E. Masunov, F. E. Hernández, *J. Phys. Chem. B* **2008**, 112, 929.
34. P. B. Johnson, R. W. Christy, *Phys. Rev. B* **1972**, 6, 4370.
35. R. Crecca, and A. R. Roitberg, *J. Phys. Chem. A* **2006**, 110, 8188.
36. M. Poprawa-Smoluch, J. Baggerman, H. Zhang, H. P. A. Maas, L. D. Cola, A. M. Brouwer, *J. Phys. Chem. A* **2006**, 110, 11926.
37. A. R. Armstrong, J. Clarkson, W. E. Smith, *J. Phys. Chem.* **1995**, 99, 17825.
38. N. Biswas S. Umapathy, *J. Phys. Chem. A* **1997**, 101, 5555.
39. C. M. Stuart, R. R. Frontiera, R. A. Mathies, *J. Phys. Chem. A* **2007**, 111, 12072.
40. N. Biswas, and S. Umapathy, *J. Phys. Chem. A* **2000**, 104, 2734.

41. A. M. Nowak and R. L. McCreery, *J. Am. Chem. Soc.* **2004**, 126, 16621.

42. A. Minisini, G. Messager, I. Piyanzina, N. Delorme, J.-F. Bardeau, *J. Struct. Chem.* **2014**, 55, 843.

43. T. J. Dines, L. D. MavGregor, C. H. Rochester, *J. Raman Spectrosc.* **2007**, 38, 832.

44. W. C. Tsoi, D.T. James, J.S. Kim, P.G. Nicholson, C.E. Murphy, D. D.C. Bradley, J. Nelson, J.-S. Kim, *J. Am. Chem. Soc.* **2011**, 133, 9834.

45. V. Hernandez, C. Castiglioni, M. Del Zoppo, G. Zerbi, *Phys. Rev. B* **1994**, 50, 9815.

46. G. M. do Nascimento, M. L. A. Temperini, *J. Raman Spectrosc.* **2008**, 39, 772.

47. Lee, J. H. Kang, I. Jo, D. Shin, B. H. Hong, *Phys. Chem. Chem. Phys.*, **2016**, 18, 3413.

48. K. Kim, J.-Y. Choi, K. S. Shin, *J. Phys. Chem. C* **2015**, 119, 5187.

49. Y. S. Yamamoto, T. Ito, J. Raman Spectrosc. **2016**, 47, 78.

50. J. R. Lombardi, R. L. Birke, T. Lu, J. Xu, *J. Chem. Phys.* **1986**, 84, 4174.

51. J. R. Lombardi, R. L. Birke, *J. Phys. Chem. C* **2008**, 112, 5605.

52. Y. Yamamoto, Y. Ozaki, T. Ito, *J. Photochem. Photobio. C: Photochem. Rev.* **2014**, 21, 81.

Graphical Abstract

<Title>
Nonresonant and resonant surface-enhanced Raman scattering of *N*-ethyl-*N*-(2-hydroxyethyl)-4-(4-nitrophenylazo) aniline in poly (methyl methacrylate) on Ag films with surface roughness

<Authors' names>
Ayaka Izumi, Kentaro Kumaoka, Masaru Shimomura, and Atsushi Sugita

<Summary>
SERS and SERRS were studied for Disperse Red 1 in poly (methyl methacrylate) on Ag films with surface roughness. The mechanisms triggering the enhancements of the Raman cross sections was discussed in terms of the electromagnetic as well as metal-to-molecule charge transfer effects by using energy diagram determined by UV-VIS absorption and UPS spectroscopies.

<Diagram>